J. Fluid Mech. (2007), *vol.* 592, *pp.* 117–133.
doi:10.1017/S0022112007008373 Printed in the United Kingdom

Strong interactions between two corotating quasi-geostrophic vortices

ROSS R. BAMBREY, JEAN N. REINAUD AND DAVID G. DRITSCHEL

Mathematical Institute, University of St Andrews, North Haugh, St Andrews, Fife KY16 9SS, UK

(Received 14 September 2006 and in revised form 13 July 2007)

In this paper we investigate the interaction between two corotating quasi-geostrophic vortices. The initially ellipsoidal vortices are separated horizontally by a distance corresponding to the margin of stability, as determined from an ellipsoidal analysis. The subsequent interaction depends on four parameters: the vortex volume ratio, the vertical centroid separation, and the height-to-width aspect ratios of each vortex. The most commonly observed strong interaction is partial merger, where only part of the weaker vortex is incorporated into the stronger one or cast into filamentary debris. Despite the proliferation of small-scale filamentary structure during many vortex interactions, on average the self-induced vortex energy exhibits an 'inverse cascade' to larger scales, broadly consistent with spectral theories of turbulence. Curiously, we observe that a range of intermediate-scale vortices are preferentially sheared out during the interactions, leaving two main populations of large and small vortices.

1. Introduction

The complex fluid motions within planetary atmospheres and oceans may aptly be described as turbulent. This turbulence results from highly nonlinear interactions between coherent swirling masses of fluid or vortices. Vortices are ubiquitous features in such 'geophysical' flows, see e.g. Holton *et al.* (1995), Garrett (2000), Marcus (1988). In the oceans, for example, Ebbesmeyer *et al.* (1986) estimated that between 10^3 and 10^4 vortices populate the surface layer of the North Atlantic alone. This turbulent motion, however, is greatly affected by the planetary rotation and the stable density stratification. This qualitatively alters the nature of turbulence, reducing the effects of vortex stretching, and rendering the flow quasi-two-dimensional. Moreover, rotation and stratification make it useful to regard vortices as coherent masses of potential vorticity, a conserved material tracer in the absence of diabatic effects and viscous dissipation. These effects are often weak on the space and time scales characteristic of geophysical turbulence.

Vortex interactions are the key ingredient in the turbulent evolution of geophysical flows, but, by their very nature, such interactions are strongly nonlinear, and thereby challenging to understand. As a result vortex interactions have been primarily studied in two-dimensional flows (relevant to motions having horizontal scales L larger than the Rossby deformation length $L_D = NH/f$, where N is the buoyancy frequency, H is the characteristic fluid depth and f is the Coriolis frequency, see Dritschel *et al.* 1999). Much of this research has attempted to explain, in physical space by the growth of vortices through merger, the average inverse energy cascade seen in two-dimensional turbulence in spectral space. Initially, the interaction between two

identical vortices was considered. Waugh (1992) identified three different types of interactions: merger, pulsation with exchange and pulsation using the terminology of Melander, Zabusky & McWilliams (1992). These types of interaction are comparable to the interaction regimes defined in Reinaud & Dritschel (2002) in the three-dimensional context (see below), with merger corresponding to complete merger, pulsation with exchange corresponding to either partial merger or weak exchange depending upon the volume of potential vorticity (PV) transferred, and pulsation corresponding to elastic interaction. Waugh (1992) also found the generation of filaments a common occurrence in vortex interactions. The work of Waugh (1992) was generalized in Dritschel & Waugh (1992) to vortices of different size. In this case, four interaction regimes were found, and most importantly complete merger was found to be surprisingly uncommon. In general, vortex interactions were frequently found to produce smaller vortices, making the association with spectral cascade theories at best tenuous. Dritschel (1995) investigated the interactions of non-circular steadily corotating vortices and demonstrated that strong interactions arise from a linear instability of the basic vortex configuration. Again complete vortex merger was found to be rare, and smaller vortices were often produced.

In the more realistic three-dimensional context, the simplest approach to simulating vortex interactions under geophysical conditions employs the quasi-geostrophic model. This model contains the dominant effects of the stable stratification and the rapid rotation of the Earth. It conveniently reduces the full equations to a single dynamical equation expressing material conservation of the PV anomaly and a simple linear inversion relation for the recovery of the velocity field. The model is based on the hydrostatic and geostrophic approximations, which neglect the fluid acceleration (in the rotating frame of reference) in the momentum equations. These approximations are valid so long as the Rossby and Froude numbers are sufficiently small (i.e. the background rotation and stratification are sufficiently strong), see Gill (1982). In the quasi-geostrophic (QG) model, the PV anomaly (hereinafter referred to as PV for simplicity) represents the departure of the full PV field from the background PV field associated with the planetary rotation in the stratified fluid, see Hoskins, McIntyre & Robertson (1985). The (geostrophic) fluid advection in QG flows is constrained to be parallel to isopycnals — i.e. layer-wise two-dimensional — though the PV distribution is fully three-dimensional.

Two-dimensional and QG flows are in fact closely analogous. The inverse energy cascade also occurs in QG turbulence, and appears to exhibit the same spectral form. Hua & Haidvogel (1986) have verified a theoretical prediction made by Charney (1971) of an inverse energy cascade in QG turbulence by demonstrating that PV forms isolated structures in both forced and freely evolving QG turbulence. Two-dimensional and QG flows also exhibit the same mathematical regularity, see Tran & Dritschel (2006).

Recent studies of vortex interactions in QG flows include works by von Hardenberg *et al.* (2000), Dritschel (2002), Reinaud & Dritschel (2002), Reinaud, Dritschel & Koudella (2003) and Reinaud & Dritschel (2005). The studies of von Hardenberg *et al.* (2000) and Dritschel (2002) focused on the influence of the vortex shape, i.e. its height-to-width aspect ratio, on the critical merger distance between horizontally aligned, equal-volume, equal-PV vortices. Dritschel (2002) found that the the merger of tall vortices does not tend to two-dimensional merger. Instead, the vortices break up into three-dimensional structures, due to a basic instability affecting tall vortices (after the conventional f/N scaling of the vertical coordinate), see Dritschel & de la Torre Juárez (1996), Dritschel, de la Torre Juárez & Ambaum (1999) and Billant, Dritschel & Chomaz (2006). Reinaud & Dritschel (2002) investigated the effects of a vertical offset on the merger distance between two vortices of equal PV, equal volume

and unit height-to-width aspect ratio (after the f/N scaling). It was discovered that vertically offset vortices can actually merge from greater horizontal separations due to the effects of vertical shear. On the other hand, in simulations of freely-decaying QG turbulence, Reinaud *et al.* (2003) demonstrated that the most robust, long-lived vortices have a mean height-to-width aspect ratio of approximately 0.8, vertical shear being responsible for the oblate vortex shape. Reinaud & Dritschel (2005) performed a linear-stability analysis to determine the critical merger distance between two equal PV ellipsoidal vortices, as a function of the volume ratio of the ellipsoids, their vertical offset and their height-to-width aspect ratios. To probe this large parameter space, Reinaud & Dritschel (2005) used a vastly-reduced model, the 'ellipsoidal model' (ELM), described in Dritschel, Reinaud & McKiver (2004), which represents vortices as uniform-PV ellipsoids, neglecting higher-order non-ellipsoidal deformations. The ELM nevertheless accurately approximates the critical merger distance, based on comparisons with the full QG model, see Reinaud & Dritschel (2005).

Due to the high computational cost of performing accurate three-dimensional QG simulations, von Hardenberg *et al.* (2000), Dritschel (2002) and Reinaud & Dritschel (2002) examined a relatively small parameter space in the entire space of vortex interactions. In the present study, we explore this space much more widely, quantifying the results of a large variety of vortex interactions. First, the ELM is used to find the vortex configurations on the approximate margin of stability, as in Reinaud & Dritschel (2005). Then, marginally unstable configurations are studied by direct numerical simulation, using the contour-advective semi-Lagrangian algorithm (CASL), described in Dritschel & Ambaum (1997). We focus on the height-to-width aspect ratio of both vortices, the vertical offset of the vortex centres and the vortex volume ratio. We restrict our analysis to vortices having equal, uniform PV. Arguably, vortices of near equal PV are the most likely to produce strong interactions.

In § 2 we provide a brief description of the quasi-geostrophic model and the associated equations. We discuss the initial conditions in § 3 along with the numerical simulation parameters. We present our results in § 4 and draw conclusions and discuss future developments in § 5.

2. The quasi-geostrophic model

The inviscid quasi-geostrophic (QG) model may be obtained from an asymptotic expansion of Euler's equations for $\epsilon = H/L \ll 1$, where H and L are characteristic height and length scales, and for $Fr^2 \ll Ro \ll 1$, where Fr and Ro are the Froude and Rossby numbers respectively. The Froude number Fr may be defined as the ratio of a characteristic horizontal vorticity to the buoyancy frequency N, while the Rossby number may be defined as the ratio of a characteristic vertical vorticity to the Coriolis frequency f. Details may be found in, e.g., Gill (1982).

For constant N and f, following many previous studies, we may stretch the vertical coordinate z by Prandtl's ratio N/f, removing any explicit dependence on N and f in the equations. Furthermore, upon neglecting relatively weak dissipative and diabatic effects, the governing equations reduce to

$$\frac{\mathrm{D}q}{\mathrm{D}t} = \frac{\partial q}{\partial t} + (\boldsymbol{u}\cdot\nabla)q = 0, \tag{2.1}$$

$$\nabla^2\psi = q, \tag{2.2}$$

$$\boldsymbol{u} = \left(-\frac{\partial\psi}{\partial y}, \frac{\partial\psi}{\partial x}, 0\right), \tag{2.3}$$

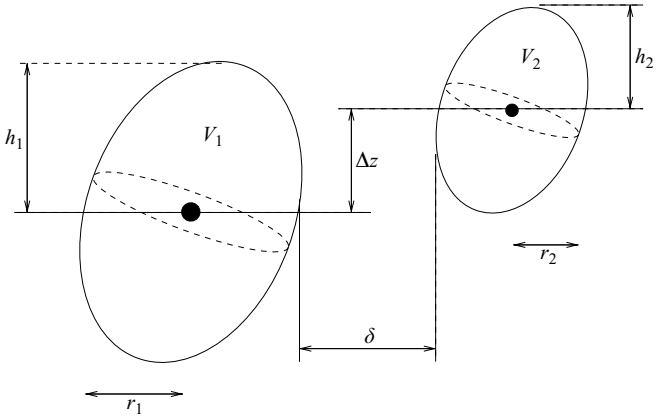

FIGURE 1. Geometry of initial conditions.

where $q(x, y, z, t)$ is the potential vorticity (PV), ψ is the streamfunction and $\boldsymbol{u}$ is the velocity. The flow is layerwise two-dimensional due to the lack of vertical advection although Poisson's equation (2.2) is isotropic.

We use the contour-advective semi-Lagrangian (CASL) algorithm to solve these equations. PV is materially conserved (by 2.1), and for the piecewise-uniform distribution considered here, the PV field can be represented entirely by contours lying on horizontal surfaces. These contours remain at all times within these surfaces. The velocity field $\boldsymbol{u}$ is obtained by inverting the Laplacian ∇^2 in spectral space. A full discussion of the CASL algorithm can be found in Dritschel & Ambaum (1997).

3. Initial conditions

We investigate pairs of corotating vortices of uniform and equal PV (set to $q = 2\pi$ without loss of generality) situated at the margin of stability. Reinaud & Dritschel (2005) computed families of (relative) equilibria for two corotating vortices within the ellipsoidal model (ELM). In that model, vortices are modelled by ellipsoids of uniform PV and any small, higher-order, non-ellipsoidal deformations are filtered, see Dritschel *et al.* (2004), Reinaud & Dritschel (2005). Each family of equilibria consists of vortices having a prescribed volume ratio, height-to-width aspect ratios and vertical offset. Members of each family differ only in their horizontal separation, most conveniently measured by the horizontal gap δ between the two innermost edges of the vortices. Vortices well separated in the horizontal have only a weak influence on one another and such equilibria are always stable. Below a critical distance or gap δ, the equilibria become unstable, making possible strong interactions such as vortex merger in the full, nonlinear QG equations.

We use in this study the first unstable equilibrium obtained as the initial conditions for the CASL simulations. This equilibrium is not *stricto sensu* an equilibrium of the full QG equations solved by CASL, yet provides an accurate estimate for it at minimal computational cost. The determination of the full equilibra, as done in Reinaud & Dritschel (2002) is simply impossible for the large parameter space considered here. The basic geometry of the flow is presented in figure 1 where the vortex ellipsoids have vertical half-heights h_i, volumes V_i and horizontal radii r_i, where $i = 1, 2$ corresponds to each vortex; they are separated by δ in the horizontal and offset by Δz in the

Parameter	Min	Max	Step
h_1/r_1	0.4	1.2	0.2
h_2/r_2	0.4	1.2	0.2
ρ_V	0.2	1.0	0.2
$\Delta z/(h_1+h_2)$	0.0	0.8	0.2

TABLE 1. Range of parameters considered in this study. Here h_i/r_i, $i=1,2$ is the height-to-width aspect ratio of each vortex, ρ_V is the volume ratio V_2/V_1 and $\Delta z/(h_1+h_2)$ the vertical offset.

vertical. We define $\rho_V = V_2/V_1$ as the volume ratio between the two vortices. The range of parameters considered is listed in table 1.

In a few cases, Reinaud & Dritschel (2005) were unable to determine the margin of instability, due to the presence of an unphysical oscillatory mode for certain horizontally-aligned equilibria. To fill this hole in the parameter space, we carried out a procedure similar to that in Reinaud & Dritschel (2005) starting from another family with a vertical offset of $\Delta z = 0.2$. Then, rather than decreasing the gap δ, we decreased Δz to zero. From there, we decreased δ, and in most cases the margin of instability could then be found. In rare cases it was necessary to use a more accurate representation of the external streamfunction of the ellipsoids by increasing the number of internal singularities (from 7 to 13) used to approximate the streamfunction (details may be found in Dritschel *et al.* 2004). This has a insignificant effect on the vortex shape characteristics, but allows one to circumvent the oscillatory mode, see Reinaud & Dritschel (2005).

In Reinaud & Dritschel (2005), the length scale of the problem was fixed by setting the total volume of the vortices to $4\pi/3$. To minimize periodicity effects in the CASL numerical simulations (see Dritschel & Macaskill 2000), we shrink the vortices so that they fit within a 2^3 box centred at the origin in the $(2\pi)^3$ computational domain with periodic boundary conditions, as in Reinaud & Dritschel (2002). We rescale distances back to their original dimensions for diagnosis in order to ensure that all vortex configurations have identical total circulation. All simulations were performed using a basic grid of resolution 64^3, with PV contours resolved down to a scale of a tenth of the grid spacing, as normal (see Dritschel & Ambaum 1997).

4. Results

4.1. *Comparison of interactions*

Each case defined in table 1 was simulated using the CASL algorithm for 60 time units. For reference, an isolated spherical vortex of uniform PV q has a rotation period of $T = 6\pi/q = 3$ here. Overall we simulated 625 cases.

We classify the interactions in each simulation following the procedure of Dritschel & Waugh (1992). By calculating the ratio of the vortices' final volumes to their initial volumes we can determine which type of interaction has taken place. Defining $\hat{V}_1 = V_{f1}/V_{i1}$ and $\hat{V}_2 = V_{f2}/V_{i2}$, where V_i and V_f are respectively the initial and final vortex volumes, the interaction types are classified according to table 2.

We identify vortices simply as contiguous regions of PV in the three-dimensional space. The procedure does not use an additional criterion, and therefore is not biased on a particular perceived view of a 'vortex'. While this implies that 'filaments' may be classified as 'vortices', experience shows that most of the structures identified this

Merger type	$\hat{V}_1$	$\hat{V}_2$
Elastic interaction (EI)	1	1
Partial straining out (PSO)	1	<1
Complete straining out (CSO)	1	0
Partial merger (PM)	>1	<1
Complete merger (CM)	>1	0

TABLE 2. Criteria for classification of vortex interactions. In EI, there is no volume change, in PSO part of one vortex is torn away and is elongated into filamentary structures, in CSO one entire vortex is elongated into filamentary structures, in PM one vortex incorporates part of the other (but both vortices survive), and in CM only one vortex survives after incorporating either all or part of the other.

way, especially at late times, have characteristics commonly associated with a 'vortex', i.e. having shapes not severely distorted from spherical.

We find that for $\rho_V = 0.2$, 92 % of the cases fall under the partial straining out (PSO) regime with the remaining 8 % being partial merger (PM). For higher volume ratios, the interactions are predominantly PM. For $0.4 \leqslant \rho_V \leqslant 1.0$, 85.8 % of the cases are PM, 9.8 % of cases are PSO, and 4.4 % of cases are complete merger (CM). Of the cases that result in complete merger, 72.7 % of these occur for cases where $\rho_V = 1.0$ and (the same) 72.7 % occur where $h_1/r_1 = h_2/r_2$. Partial straining out does not occur at all for the equal-volume vortices in this parameter space. No instances of complete straining out (CSO) or elastic interactions (EI) are seen in this parameter space.

In figure 2 we show four time frames from an interaction in a partial straining out regime. The initial conditions are $h_1/r_1 = 0.8$, $h_2/r_2 = 1.0$, $\rho_V = 0.2$ and $\Delta z = 0.2$. At time $t = 7$ filaments begin to be stripped away from the smaller vortex. These filaments orbit the larger vortex but do not merge with it. By $t = 60$ the smaller vortex has lost 5 % of its original volume and now has $h/r = 0.92$. The volume and aspect ratio of the larger vortex have remained unchanged throughout.

The simulation displayed in figure 3 has initial conditions $h_1/r_1 = 1.0$, $h_2/r_2 = 0.4$, $\rho_V = 1.0$ and $\Delta z/(h_1 + h_2) = 0.2$. In this case the volume of PV transferred between the vortices is sufficient to classify the interaction as partial merger. At $t = 7$ the two initial vortices temporarily merge into a 'dumbbell' shaped configuration with an effective h/r of 0.58. At $t = 13$ the dumbbell vortex begins to eject filaments (see figure 4 for an alternative view at $t = 14$), and at $t = 21$ it splits into two large scale vortices with a volume ratio of 0.53. The larger of these vortices has $h/r = 0.79$ and the smaller has $h/r = 0.57$. It is apparent that these small-scale structures are ejected by the larger vortex between $t = 21$ and $t = 40$ as its volume at $t = 40$ is 91 % of what it was at $t = 21$. The smaller vortex, on the other hand, has grown by 0.4 % during this time. At $t = 60$ the number of structures present has decreased. At this final time the larger vortex has grown by 2 % over its original volume at $t = 21$ whereas the smaller vortex has 2 % less volume than at $t = 21$. The ending volume ratio of these two main vortices is 0.56.

One other interesting example is shown in figure 5. On first inspection one would expect this interaction to belong in the complete-merger regime and indeed it displays behaviour like that described in Waugh (1992) for complete-merger where the central vortex elliptical shape has an aspect ratio greater than 3. However, using the criteria set out in table 2 this interaction is classified as partial-merger due to the large quantity of filaments ejected. The initial vortices merge by $t = 2$ forming a central vortex of $h/r = 0.97$. Figure 5(*b*) shows filaments forming at both vertical apexes

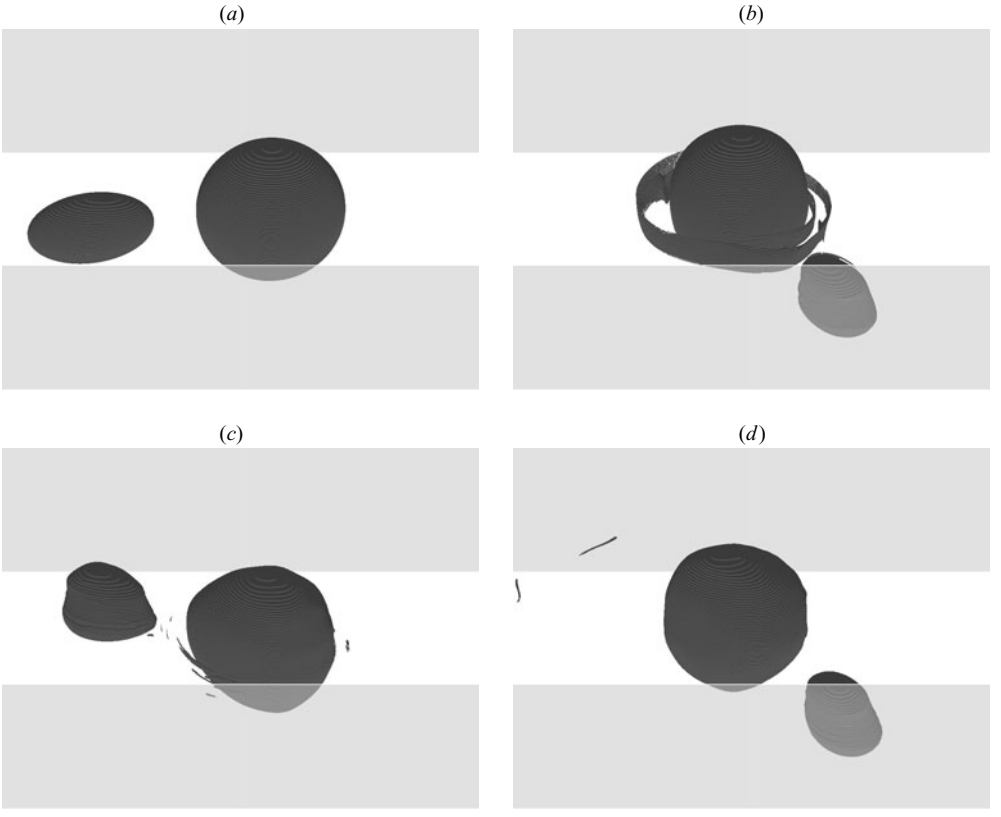

FIGURE 2. Vortex evolution in a PSO regime. $h_1/r_1 = 0.8$, $h_2/r_2 = 1.0$, $\rho_V = 0.2$ and $\Delta z = 0.2$. Time frames shown are (*a*) $t = 0$, (*b*) $t = 14$, (*c*) $t = 40$ and (*d*) $t = 60$. The viewing angle is 60° from the vertical and the horizontal scale is ± 1.5 centred around the origin of the domain. Light-grey areas show the front and back walls of the box which span the full height of the PV distribution.

of the central vortex at $t = 14$. At $t = 16$ these filaments begin to separate from the central vortex. By $t = 40$ the central vortex has reduced to 90 % its volume at $t = 2$ and its aspect ratio h/r has reduced to 0.89. At the final time, $t = 60$, the central vortex has further decreased in volume to 81 % of that at $t = 2$ and its h/r is now 0.81. A near vertical view of the PV at this time is shown in figure 6 — note in particular the formation of vortices occurring in the outer filaments, where the strain of the central vortex is too weak to prevent vortex roll-up.

4.2. *Analysis over entire parameter space*

Individual cases exhibit a wide variety of behaviour and significant complexity. We next examine the parameter space as a whole, and look for trends in certain statistics to understand better general aspects of vortex interactions.

An important feature of geophysical turbulent flows is the on-average cascade of energy to large scales — in spectral space. To determine if an analogous cascade occurs in physical space, we diagnose the vortex self-energy E_s

$$E_s = -\frac{1}{2}\iiint q\psi \, \mathrm{d}V \tag{4.1}$$

at various times during each interaction. In the above, ψ is the streamfunction induced by the vortex on itself. Note that, generally, the total energy is dominated by the

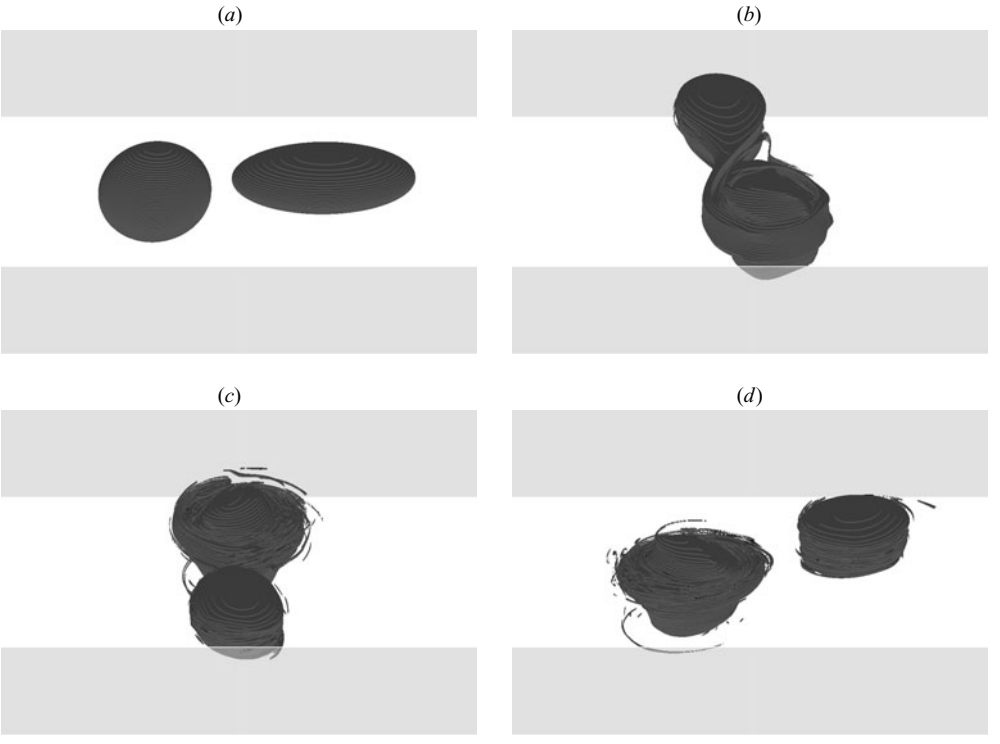

FIGURE 3. Vortex evolution in a partial-merger (PM) regime. $h_1/r_1 = 1.0$, $h_2/r_2 = 0.4$, $\rho_V = 1.0$ and $\Delta z = 0.2$. Time frames shown are (*a*) $t = 0$, (*b*) $t = 14$, (*c*) $t = 40$ and (*d*) $t = 60$. The viewing angle is 60° from the vertical and the horizontal scale is ± 1.5 centred around the origin of the domain. Light-grey areas show the front and back walls of the box which span the full height of the PV distribution.

sum of vortex self-energies as the vortex interaction energy is relatively small, see Reinaud & Dritschel (2005).

Figure 7 shows the number of vortices of a given self-energy E_s and mean radius r, with $r = (3V/4\pi)^{1/3}$, taken over the entire parameter space at times $t = 0$, 30, 40 and 60. Note in particular the very large number of small-scale vortices generated during the interaction processes, as seen in the specific examples presented in figures 3 and 5.

The energy distribution, particularly for large vortices and to some extent the smallest vortices, is well approximated by $E_s = (4\pi Q^2/15)r^5$, the energy of a *spherical* vortex of uniform PV, Q. One would expect such a power-law dependence from (4.1), but it is striking just how well the data are fit by the energy of a spherical vortex. A noticeable gap develops in the range $10^{-0.6} \approx 0.25$ to $10^{-0.4} \approx 0.40$. Energy levels for vortices in this range at earlier times are significantly lower than those of spherical vortices of the same volume. This indicates that the vortices are strongly deformed, and as time proceeds, appear to be sheared out or reabsorbed by the larger vortices.

To determine what happens to the vortices in this range, we plot the mean radius of all of the largest vortices versus time in figure 8. This shows that there is no growth of the largest vortex at later times, hence it follows that the vortices in the range $0.25 \leqslant r \leqslant 0.40$ are destroyed by shear effects from the larger vortices.

Interestingly, the same shear effects do not destroy the smallest vortices. This appears to be related to the fact that small vortices can move further away from the main vortex or vortices while maintaining conservation of angular momentum.

FIGURE 4. Near vertical view of the dumbbell vortex at $t = 14$ in figure 3 (the viewing angle is 10° from the vertical).

Essentially, thin filaments may be ejected to greater distances initially than the wider filaments of PV, as is clearly evident from figure 5, for example. These thin filaments then roll up into small vortices, while the larger filaments must battle the stronger shear of the larger vortices to survive. The larger vortices effectively remove all other vortices in close proximity.

Judging by the apparently even spacing between contours for smaller vortices in figure 7 it appears that the number density is related to the vortex radius by a power law. We confirm this in figure 9, which shows that the number density $n(r)$ for small vortices approximately follows $n \propto r^{-4}$, indicated in the figure by a reference line. For widely separated vortices, when the energy is dominated by the vortex self-energies, this r^{-4} number density distribution corresponds in spectral space to a k^{-3} energy spectrum (identifying k with r^{-1}), which is the classical small-scale energy spectrum predicted by Charney (1971) for quasi-geostrophic turbulence. This follows by equating the energy density $n(r)E_s(r)\,\mathrm{d}r$ with $E(k)\,\mathrm{d}k$. Finally, it is also worth noting that despite the enormous quantity of small vortices, the volume of vortices with radius $\log_{10} r < -0.325$ (i.e. $r < 0.473$) is only 0.8 % of the total volume of vortices.

We next investigate how the vortex self-energy is redistributed during the interactions. Figure 10 shows the result of integrating the self-energy displayed in figure 7(*a*) and 7(*d*) with respect to vortex radius. Here F, defined by

$$F(r) = \frac{1}{n}\int_0^r E_s(r')\,\mathrm{d}r',$$

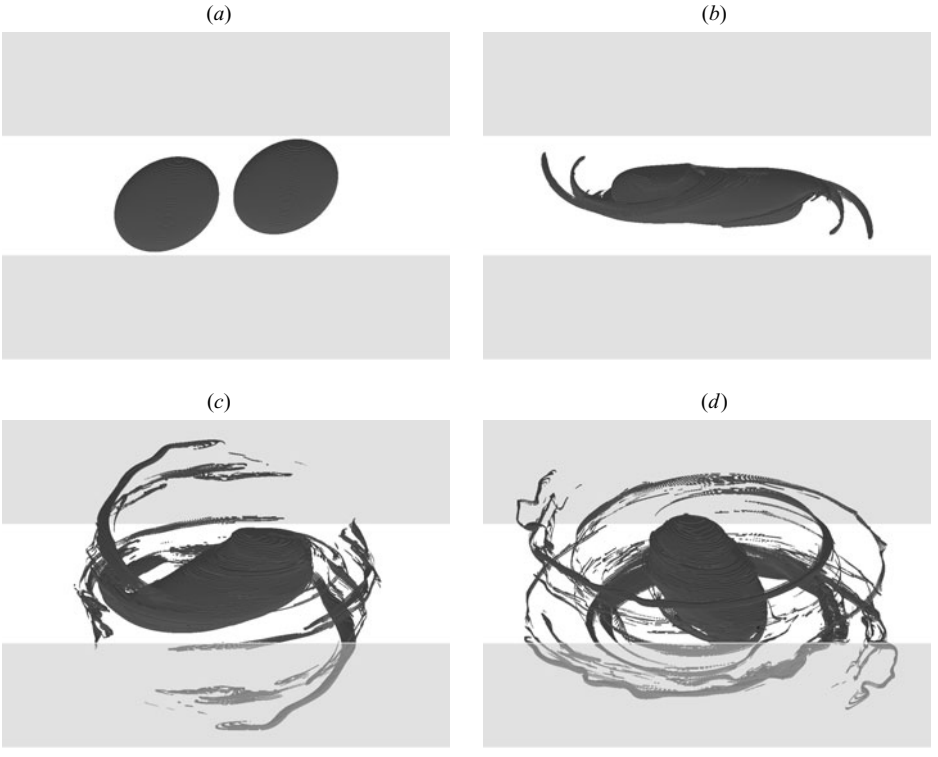

FIGURE 5. Vortex evolution in a partial-merger (PM) regime. $h_1/r_1 = 1.2$, $h_2/r_2 = 1.2$, $\rho_V = 1.0$ and $\Delta z = 0.2$. Time frames shown are (*a*) $t = 0$, (*b*) $t = 14$, (*c*) $t = 40$ and (*d*) $t = 60$. The viewing angle is 60° from the vertical and the horizontal scale is ± 2.0 centred around the origin of the domain. Light-grey areas show the front and back walls of the box which span the full height of the PV distribution.

gives the amount of energy contained in all vortices up to scale r (normalized by the number of simulations, $n = 625$). The $t = 60$ curve in figure 10 is arranged in two distinct parts. There is an initial increase in $F(r)$ between $r = 0.5$ and $r = 0.76$ corresponding to the smaller vortices and filaments created during the interactions. The larger vortex from partial-merger events and the main vortex from complete-merger events occupy the steep part of the curve $F(r)$ around $r = 0.84$. This is also evident in figure 7, where a small gap occurs around $r = 0.8$. The conclusion from figure 10 is that there is an average inverse cascade of self-energy, i.e. a transfer of self-energy to larger-scale structures in physical space.

To investigate the mean energy-containing scale, we introduce the energy-weighted mean radius $\bar{r}$ at a time t by

$$\bar{r} = \frac{\sum_{i=1}^{m} E_{si} r_i}{\sum_{i=1}^{m} E_{si}}, \tag{4.2}$$

where m is the total number of vortices over the whole parameter space at a particular time t. Figure 11 shows the variation of $\bar{r}$ with time. Initially, $\bar{r}$ increases over the first 14 time units, during which interactions are predominantly merger. Afterwards,

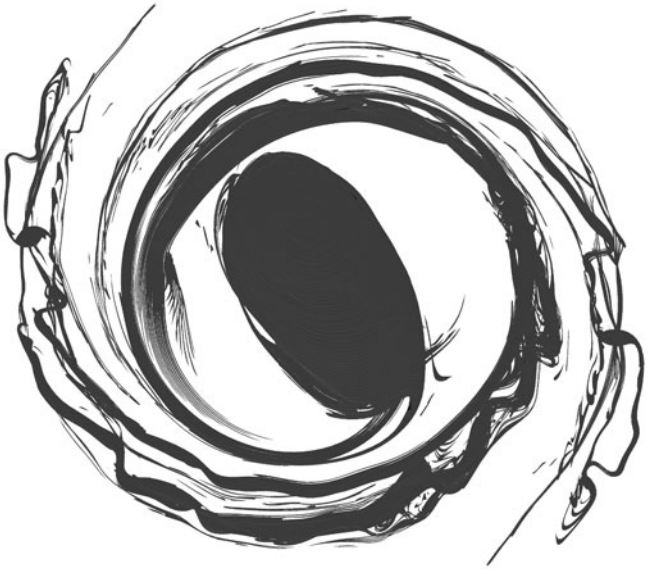

FIGURE 6. Near vertical view of the PV distribution at $t = 60$ in figure 5 (the viewing angle is 10° from the vertical).

Time (t)	E_{sl}	E_{sg}
0	10.41	11.45
14	0.73	23.83
30	2.49	20.32
40	3.09	18.84
60	3.30	17.09

TABLE 3. Values of E_{sl}, E_{sg} at times 0, 14, 30, 40 and 60.

$\bar{r}$ begins to decrease as the vortices separate and eject filaments. By $t = 50$, $\bar{r}$ has converged to $\bar{r} = 0.87$, showing that, on average, the mean vortex radius has increased by 3.5 %.

To understand better the nature of the energy transfers, we consider next the mean self-energy E_{sl} of vortices whose radius is less than $\bar{r}_0$ ($\bar{r}$ at $t = 0$), and similarly the mean self-energy E_{sg} of vortices whose radius is greater than $\bar{r}_0$. Figure 12 plots the ratio E_{sl}/E_{sg} versus time (E_{sl} and E_{sg} are listed separately in table 3). The ratio of mean energies decreases rapidly at early times, once again indicating an 'inverse cascade' of the self-energy towards larger scales. However, E_{sl}/E_{sg} begins to increase at about $t = 14$, just when small-scale structures begin to be ejected, and when 'merger' becomes a poor characterization of typical interactions. By $t = 60$, 70 % of the vortex self-energy is contained in structures whose mean radius is greater than $\bar{r}_0$.

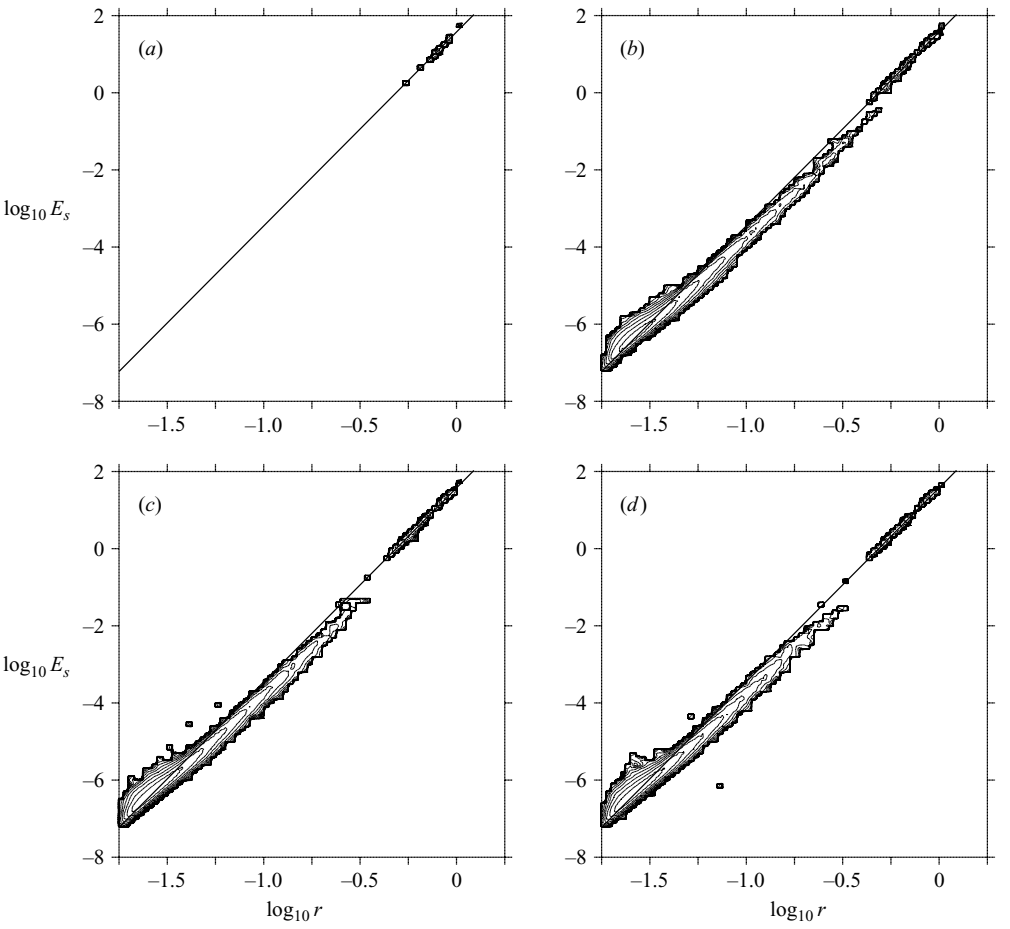

FIGURE 7. Contours of the number density (n) of vortices (contoured as $\log_{10} n$). The first (outermost) contour has $\log_{10} n = 0$, the innermost contour has $\log_{10} n = 11$, the contour increment is $\log_{10} \Delta n = 0.5$. 100 intervals were used in each direction, equally spaced in logarithmic scales. We add for reference the line corresponding to the energy of a sphere of PV Q, $E_s = (4\pi Q^2/15) r^5$.

In figure 13 we show how the mean radius of the largest vortex at the end of evolution depends on the initial volume ratio. We find that the closer the initial volume ratio is to unity, the larger the main final vortex tends to be and hence the greater its self-energy. A high degree of variance is seen for $\rho_V = 1.0$, and the size of this error bar is not dependent on the vertical offset as a similarly high variance is seen for $\rho_V = 1.0$ when averaging only over h/r for each value of Δz.

5. Conclusions

In this paper we have investigated the interactions between two corotating quasi-geostrophic vortices of varying height-to-width aspect ratios, volume ratios and vertical offsets separated in the horizontal so that they reside at the approximate margin of stability.

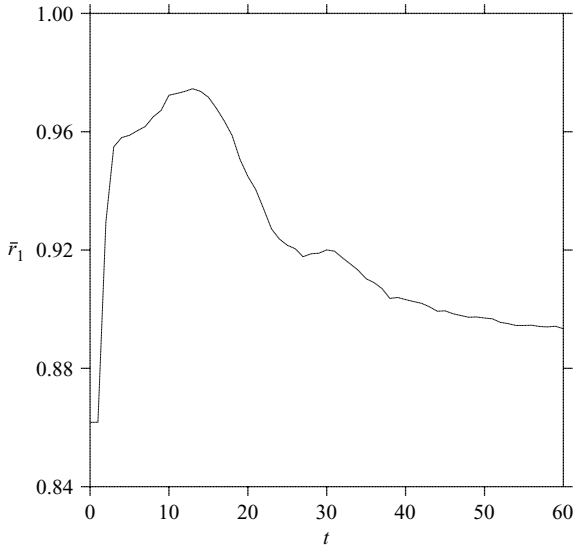

FIGURE 8. Mean radius of the largest vortex against time, with the radius averaged over all cases.

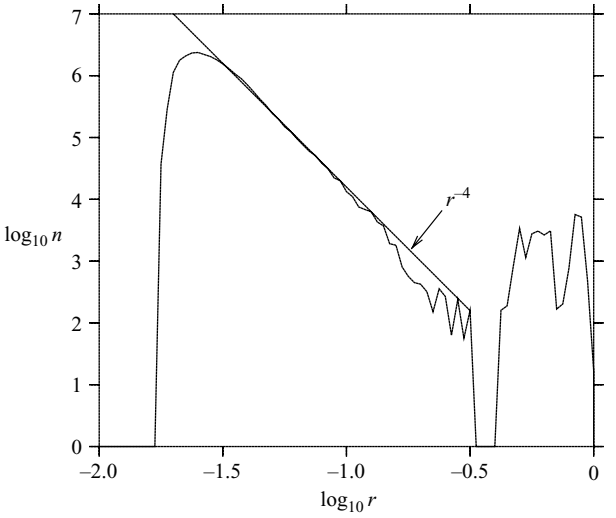

FIGURE 9. Number density of vortices as a function of the radius. As in figure 7 we use 100 intervals in the direction of $\log_{10} r$. This is at $t = 60$. We add for reference the slope r^{-4}, which corresponds to an energy spectrum $E(k) \propto k^{-3}$ for widely separated vortices.

We find that for the smallest volume-ratio interactions considered ($\rho_V = 0.2$), the evolution is most likely to fall into the partial straining out regime, where the smaller vortex becomes smaller by losing filaments while the larger vortex remains unchanged. For larger volume ratios, between 0.4 and 1.0, interactions are more likely to be partial mergers, where part of the smaller vortex is incorporated into the larger one. In the parameter space considered, we find that the classical picture of vortex merger, i.e. complete merger, is extremely rare and results almost exclusively from interactions between vortices of equal volume and height-to-width aspect ratio. Perhaps most

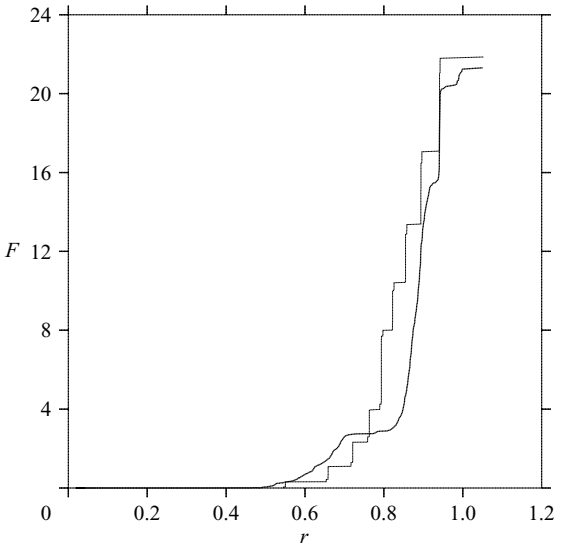

FIGURE 10. $F(r) = (1/n)\int_0^r E_s(r')\,\mathrm{d}r'$ plotted against r, where $n = 625$ is the number of simulations, at times $t = 0$ (thin line) and $t = 60$ (bold line).

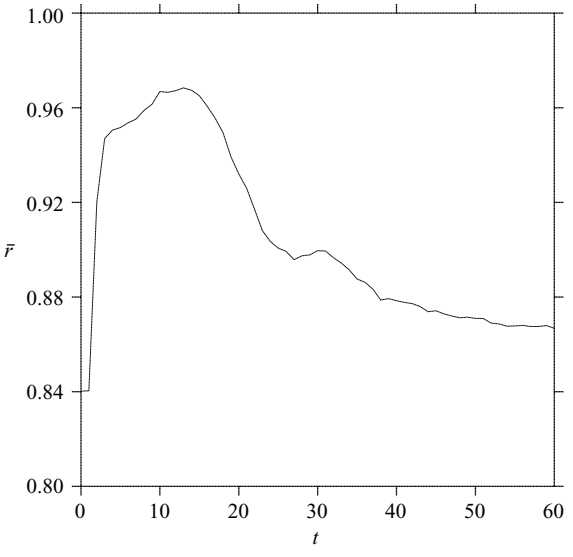

FIGURE 11. Energy-weighted mean radius($\bar{r}$) plotted against time t.

importantly, there is no significant dependence of the interaction type on the vertical offset of the vortices. This conclusion applies to the full range of vertical offsets for which vortices can potentially merge.

Over the wide-ranging initial conditions considered, the first interactions to occur between the vortices tend to be merger. Then, after about five characteristic vortex rotation periods, regardless of whether the merged pair remains together or not, a large number of small-scale filamentary structures are ejected. But despite this, the vortex self-energy exhibits an 'inverse cascade' in that, on average, self-energy is

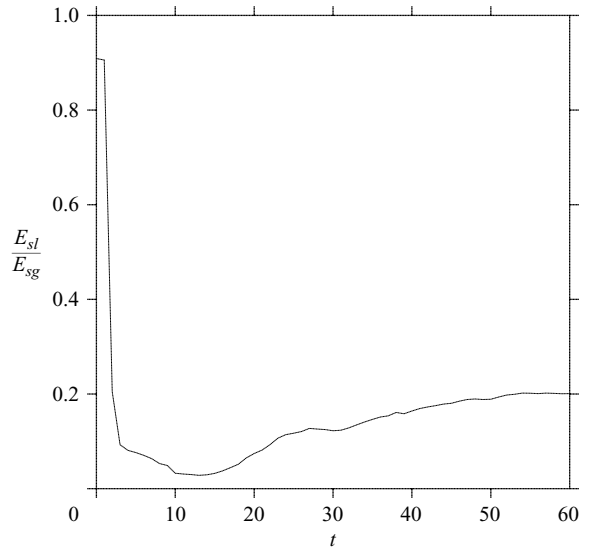

FIGURE 12. E_{sl}/E_{sg} plotted against time t

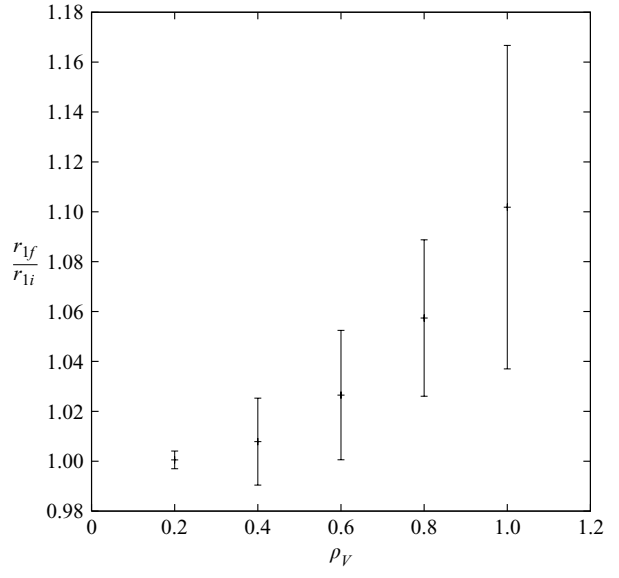

FIGURE 13. Ratio of the radius of the largest vortex at $t = 60$ (r_{1f}) to the radius of the largest vortex at $t = 0$ (r_{1i}) plotted against the initial volume ratio, ensemble-averaged over all height-to-width aspect ratios and vertical offsets.

transferred to larger physical scales over time. Vortices in an intermediate range of scales, here $r = 10^{-0.6} \approx 0.25$ to $r = 10^{-0.4} \approx 0.40$, are sheared out into filaments by the larger vortices (note: all vortex configurations have the same total circulation and volume, here $4\pi/3$). This leaves two primary vortex populations, vortices whose mean radii lie between 0.40 and 1.0 and vortices whose mean radii lie below 0.25. Almost no vortices are found between these primary populations.

The largest vortex in an interaction tends to grow by the biggest proportion when the initial vortex volume ratio is close to unity. There is, however, a high degree of variance in this growth, with the mean radius growing anywhere between 4.8 % and 17.7 %. Statistically, in a turbulent flow containing an ever increasing number of vortices with decreasing scale (see Reinaud *et al.* 2003), interactions between similarly-sized vortices are likely to be rare compared to interactions between disparate-sized vortices. Notably, the latter result in weak or no growth of the larger vortex.

This study has used the simplest model of a rotating, stratified flow, the quasi-geostrophic model, strictly valid only for small Rossby numbers and small Froude numbers. It is important in practical applications to the atmosphere and oceans to determine how these results are modified by relaxing the QG approximation, allowing ageostrophic effects and the spontaneous generation of inertia-gravity waves during vortex interactions. These effects are presently unknown.

Support for this research has come from the UK Natural Environment Research Council (grant ref. NER/S/A/2003/11903).

REFERENCES

Billant, P., Dritschel, D. G. & Chomaz, J.-M. 2006 Bending and twisting instabilities of columnar elliptical vortices in a rotating strongly stratified fluid. *J. Fluid Mech.* **561**, 73–102.

Charney, J. 1971 Geostrophic turbulence. *J. Atmos. Sci.* **28**, 1087–1095.

Dritschel, D. G. 1995 A general theory for two-dimensional vortex interactions. *J. Fluid Mech.* **293**, 269–303.

Dritschel, D. G. 2002 Vortex merger in rotating stratified flows. *J. Fluid Mech.* **455**, 83–101.

Dritschel, D. G. & Ambaum, M. H. P. 1997 A contour-advective semi-lagrangian algorithm for simulating fine-scale conservative dynamical fields. *Q. J. R. Met. Soc.* **123**, 1097–1130.

Dritschel, D. G. & Macaskill, C. 2000 The role of boundary conditions in the simulation of rotating, stratified turbulence. *Geophys. Astrophys. Fluid Dyn.* **92**, 233–253.

Dritschel, D. G., Reinaud, J. N. & McKiver, W. J. 2004 The quasi-geostrophic ellipsoidal model. *J. Fluid Mech.* **505**, 201–223.

Dritschel, D. G. & de la Torre Juárez, M. 1996 The instability and breakdown of tall columnar vortices in a quasi-geostrophic fluid. *J. Fluid Mech.* **328**, 129–160.

Dritschel, D. G., de la Torre Juárez, M. & Ambaum, M. H. P. 1999 On the three-dimensional vortical nature of atmospheric and oceanic flows. *Phys. Fluids* **11**, 1512–1520.

Dritschel, D. G. & Waugh, D. W. 1992 Quantification of the inelastic interaction of unequal vortices in two-dimensional vortex dynamics. *Phys. Fluids* A **4**, 1737–1744.

Ebbesmeyer, C. C., Taft, B. A., McWilliams, J. C., Shen, C. Y., Riser, S. C., Rossby, H. T., Biscaye, P. E. & Östlund, H. G. 1986 Detection, structure and origin of extreme anomalies in a western atlantic oceanographic section. *J. Phys. Oceanogr.* **16**, 591–612.

Garrett, C. 2000 The dynamic ocean. In *Perspectives in Fluid Mechanics* (ed. G. K. Batchelor, H. K. Moffatt & M. G. Worster), chap. 10. Cambridge University Press.

Gill, A. E. 1982 *Atmosphere-Ocean Dynamics.* Academic.

von Hardenberg, J., McWilliams, J. C., Provenzale, A., Shchepetkin, A. & Weiss, J. B. 2000 Vortex merging in quasi-geostrophic flows. *J. Fluid Mech.* **412**, 331–353.

Holton, J. R., Haynes, P. H., McIntyre, M. E., Douglass, A. R., Rood, R. B. & Pfister, L. 1995 Stratosphere-troposphere exchange. *Revs. Geophys.* **33**, 403–439.

Hoskins, B. J., McIntyre, M. E. & Robertson, A. W. 1985 On the use and significance of isentropic potential-vorticity maps. *Q. J. R. Met. Soc.* **111**, 877–946.

Hua, B. L. & Haidvogel, D. B. 1986 Numerical simulations of the vertical structure of quasi-geostrophic turbulence. *J. Atmos. Sci.* **43**, 2923–2936.

Marcus, P. S. 1988 Numerical simulation of jupiter's great red spot. *Nature* **331**, 693–696.

Melander, M. V., Zabusky, N. J. & McWilliams, J. C. 1992 Symmetric vortex merger in two dimensions: causes and conditions. *J. Fluid Mech.* **195**, 303–340.

Reinaud, J. N. & Dritschel, D. G. 2002 The merger of vertically offset quasi-geostrophic vortices. *J. Fluid Mech.* **469**, 287–315.

Reinaud, J. N. & Dritschel, D. G. 2005 The critical merger distance between two co-rotating quasi-geostrophic vortices. *J. Fluid Mech.* **522**, 357–381.

Reinaud, J. N., Dritschel, D. G. & Koudella, C. 2003 The shape of the vortices in quasi-geostrophic turbulence. *J. Fluid Mech.* **474**, 175–192.

Tran, C. V. & Dritschel, D. G. 2006 Vanishing enstrophy dissipation in two-dimensional navier–stokes turbulence in the inviscid limit. *J. Fluid Mech.* **559**, 107–116.

Waugh, D. 1992 The efficiency of symmetric vortex merger. *Phys. Fluids* A **4**, 1745–1758.